Encapsulating *N*-Heterocyclic Carbene Binuclear Transition-Metal Complexes as a New Platform for Molecular Rotation in Crystalline Solid-State

Mingoo Jin*[†‡], Rempei Ando[†], Marcus J. Jellen[¶], Miguel A. Garcia-Garibay[¶], Hajime Ito*[†‡]

[†]Division of Applied Chemistry and Frontier Chemistry Center (FCC), Faculty of Engineering, Hokkaido University, Sapporo, Hokkaido 060-8628, Japan

‡Institute for Chemical Reaction Design and Discovery (WPI-ICReDD), Hokkaido University, Sapporo, Hokkaido, 060-8628, Japan

[¶]Department of Chemistry & Biochemistry, University of California Los Angeles, California 90095-1569, United States

Crystalline molecular rotor, Solid-state luminescence

ABSTRACT: In crystalline solids, molecules generally have limited mobility due to their densely packed environment. However, structural information at the molecular level may be used to design amphidynamic crystals with rotating elements linked to rigid, lattice-forming parts, which may lead to molecular rotary motions and changes in conformation that determine the physical properties of the solid-state materials. Here, we report a novel design of emissive crystalline molecular rotors with a central pyrazine rotator connected by implanted transition metals (Cu or Au) to a readily accessible enclosure formed by two *N*-heterocyclic carbenes (NHC) in discrete binuclear complexes. The activation energies for the rotation could be tuned by changing the implanted metal. Exchanging Cu to Au resulted in a ca. 4.0 kcal/mol reduction in the rotational energy barrier as a result of lower steric demand by elongation of the axle with the noble metal, and a stronger electronic stabilization in the rotational transition state by enhancement of the *d*–□ interactions between the metal centers and the pyrazine rotator. The Cu(I) rotor complex showed a greater electronic delocalization than the Au(I) rotor complex, causing a red-shifted solid-state emission. Molecular rotation-induced emission quenching was observed in both crystals. The enclosing NHC rotors are easy to prepare, and their rotational motion should be less dependent on packing structures, which are often crucial for many previously documented amphidynamic molecular crystals. The platform from the encapsulating NHC cationic metal complexes and the metal-centered rotation-axis provide a promising scaffold for a novel design of crystalline molecular rotors, including manipulation of rotary dynamics and solid-state emission.

Introduction

Molecules in crystals are generally packed in highly dense close-packing environments and show limited atomic and molecular motion. However, design elements that generate sufficient volume near axially linked molecular rotators allow for large angular displacements, even in the solid phase (Figure 1a). With highly ordered structures and fast rotatory dynamics precisely defined at the molecular and macroscopic scales, it has been suggested that such "*amphidynamic crystals*"[1-5] are a promising platform for the development of smart materials and molecular machines.[2] In these systems, solid-state functions arise from molecular rotations and reorientations that cause anisotropic changes in most physical properties. Examples reported include materials that present useful gas adsorption/desorption[3,5], semiconducting behavior[6], tunable optics[7-8], and mechanically responsive properties[9-11,14], among several others[4,12]. In a recent example, we developed a series of luminescent amphidynamic crystals where the intensity of their solid-state phosphorescence is correlated to time-dependent changes in conjugation that result from the rotational motion of the aromatic luminophores that are part of Au(I)-containing complexes[13-14]. Crystalline molecular rotors capable of controlling physical properties by altering the molecular rotation represent a critical development in solid-state functional materials, as well as a promising strategy to transduce molecular-level functions to the macroscopic scale. However, the construction of new structural motifs to control rotary motions in solid-state remains a significant challenge.

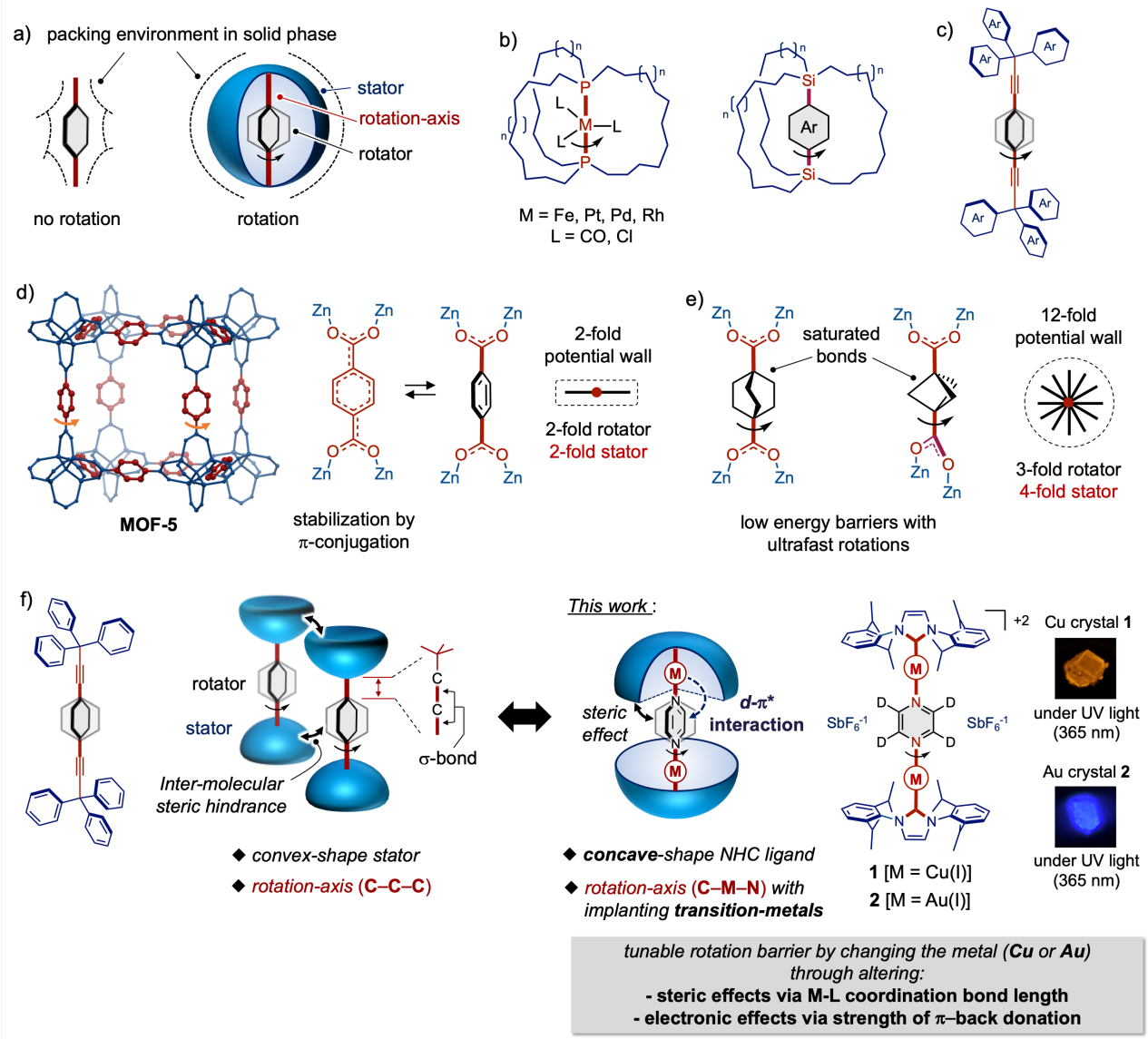

Figure 1. Crystalline molecular rotors built with a concave-shaped NHC group and the implantation of metals to rotation-axis. a) Molecular rotation and packing environment in the solid phase. b) Molecular gyroscopes constructed with a central rotator coaxially linked by an axle to two bridging stators. c) Dumbbell shape molecular rotors possessing trityl-based stator. d) MOF-5 with phenyl groups acting as rotators and linkers with high rotational barriers due to the loss of π-conjugation at the transition state. e) MOFs with saturated rotators that cycloaliphatic feature with symmetry mismatch of rotator-stator display ultrafast rotation in the solid-state. f) Representation of dumbbell-shaped molecular rotor possessing trityl group as a convex-shape stator, and the newly designed concave-shaped NHC cationic, luminescent molecular rotors 1 and 2 with Cu(I) or Au(I) metals implanted along the rotational-axis.

Gyroscope-like molecular rotors[1,2,7,15,16], dumbbell-shaped molecules[1,2], and porous materials such as metal-organic frameworks (MOFs)[3,5,12,17-21] have been employed as general platforms of amphidynamic crystals. Molecular gyroscopes possessing a functional rotator connected to an enclosing stator by triple bonds serving as the rotation axle were first proposed by Garcia-Garibay *et al.* for constructing crystalline molecular rotors.[1,2] This was followed by the development of bridged trityl-based molecular gyroscopes[15] by the same group, metal complexes with bridgehead diphosphine cages[16] by Gladysz *et al.*, and phenylene rotors shielded by bridging silyl cages[7] by Setaka *et al.* (Figure 1a and b). All these examples were shown to have rotational motion limited by intramolecular steric effects with the enclosing stators.[1,2] Unfortunately, structural optimization in these examples has been limited by the inherent difficulties in the synthesis of their multi-bridged macrocyclic structures. Efficient access to a wide range of amphidynamic crystals was shown to be possible by taking advantage of dumbbell-shaped structures with open topologies, as shown by the Garcia-Garibay group (Figure 1c)[1,2]. In this particular design, trityl stators create a convex shape around the central rotator that prevents intramolecular steric interactions, but inter-molecular steric shielding has been shown to be largely unpredictable[2].

In contrast to gyroscope-like or dumbbell-shaped close-packed molecular rotors, highly porous metal organic frameworks (MOFs) can be built with molecular rotors that have minimal steric hindrance[3,5]. In the case of arylene dicaboxylates used both as building blocks and molecular rotators in zinc-oxide and paddlewheel MOF structures, electronic barri-

ers to rotation are the result of changes in conjugation between the central phenylene rotator and the carboxylate groups that are coordinated to the metal center. In addition, the axial symmetry order of the carboxyl stator and the central-rotator affect the rotational energy profile and the height of the corresponding barriers. For example, a 1,4-phenylene-dicarboxylate rotator in MOF-5 showed relatively slow two-fold rotational motion due to a high electronic barrier (E_a=11.3±2 kcal/mol) that results from the loss of electronic conjugation at the transition state of the two-fold symmetric potential despite having a very low packing density and no steric hindrance in solid-state (Figure 1d)[17]. By contrast, non-aromatic or cycloaliphatic dicarboxylates with higher rotational symmetry have no conjugation and display a stator-rotator symmetry mismatch that results in a larger number of energy minima, such that they can have insignificant rotational barriers (E_a<0.2 kcal/mol) that result in the fastest molecular rotations (~10^{10} Hz) reported thus far in the crystalline phase, as recently demonstrated by Garcia-Garibay *et al.*[21] and by Sozzani *et al.*[22] (Figure 1e). The combination of a 4-fold symmetric stators and 3-fold symmetric bicyclo[1.1.1]pentane rotator result in 12-fold potential energy profile, which allows for the rotator to reach a GHz rotary mobility at extremely low temperature, as detected by T_1-solid-state NMR and muon spectroscopies at 2 K[22b].

Searching for a new structural entry for the development of molecular rotation in the solid-state we envisioned a semi-enclosed, encapsulating bimetallic complex rotor with a concave-shaped bulky *N*-heterocyclic carbene (NHC) stator, and an aromatic rotator co-axially coordinated to transition metals (Cu or Au) along the rotational axis (Figure 1f). The bulky concave-shaped NHC ligands have been used to design organometallic catalysts due to their shielding effects that protect the metal-center during reactions while also providing them with steric interactions that control the stereochemistry of products[23,24]. We reasoned that the shielding feature of the bulky NHC groups should shield the rotator in a manner that is similar to that of the enclosed rotators of molecules gyroscopes. At the same time, the metal-centered axle should be able to modulate the rotary motion by altering the steric hindrance and electronic interactions between the central rotator, the variable metal center, and the carbene carbon. Under these conditions, it should be possible to tune the length of the axle by altering the metal atoms as they have different sizes, while π-back donation from their filled *d* orbital to the π^* orbitals of the ligands can also be influenced by the torsional angles of the ligands[25,26]. Considering the high accessibility and structural diversity of the NHC ligands, as well as the simplicity of complex formation with various transition metals, we hypothesize that this NHC-based design will afford a promising new platform for the construction of tunable amphidynamic crystals (Figure 1f).

To explore this concept, we prepared two novel Cu(I) and Au(I) binuclear complexes bridged by deuterated pyrazine, as a rotator and internal ligand, with two 1,3-bis(2,6-diisopropylphenyl)imidazol-2-ylidene (IPr-NHC) groups at the two ends (Figure 1f). The concave-shaped IPr-NHC ligands constitute the enclosing stator while the pyrazine ring with π-accepting ability from the *d* orbitals of either Cu(I) or Au(I) metals plays the role of the central rotator. Red and blue luminescent crystals of NHC Cu(I) rotor **1** and Au(I) rotor **2**, respectively, were obtained in good yields, and were shown to have the expected structures by single-crystal X-ray diffraction (XRD). Variable temperature solid-state ^{2}H NMR confirmed that the two crystals are amphidynamic with 2-fold rotational motion. Arrhenius plots built with rotational frequencies obtained by line shape analysis revealed activation energies (E_a) of 11.0 kcal/mol and 7.6 kcal/mol for crystals of Cu(I) rotor **1** and Au(I) rotor **2**, respectively. DFT calculations revealed that the lower rotational barrier in the case of the Au(I) rotor **2** is the result of a smaller intra-molecular steric repulsion between the bulky NHC ligand and pyrazine rotator that correlates with the elongation of the axle, and a larger stabilization of the transition state by greater π-back donation from the metal to the rotator due to the increased overlap between the *d* and π^* orbitals.

Results and Discussion

Synthesis and Characterization.

Cationic Cu(I) and Au(I) molecular rotors with NHC ligands (**1** and **2**) were obtained as crystalline solids in 73% and 68% of yield, respectively, by anion exchange from deuterated pyrazine, chloro[1,3-bis(2,6-diisopropylphenyl)imidazol-2-ylidene]Cu(I) [IPrCu(I)Cl] or chloro[1,3-bis(2,6-diisopropylphenyl)imidazol-2-ylidene]Au(I) [IPrAu(I)Cl], and $AgSbF_6$ (scheme 1 and 2). Crystallizations were performed by solvent diffusion from DCM solutions of 1 or 2 into layered hexane. Crystals **1** and **2** were shown to emit red and blue luminescence, respectively, under UV light (λ=365 nm) at ambient temperature as shown in Figures 2a and 2b. Solvent inclusion was not observed by either single crystal XRD, or by thermogravimetric analysis (TGA) (Figures 2d–g and S1). Crystalline samples were characterized in solution by ^{1}H and ^{13}C NMR spectroscopy, and in the solid-state by elemental analysis, TGA, and single-crystal X-ray diffraction (XRD) (see Supporting Information).

Scheme 1. Synthesis of Cu(I) NHC rotor complex 1

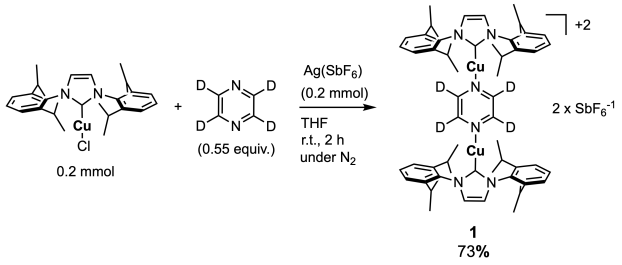

Scheme 2. Synthesis of Au(I) NHC rotor complex 2

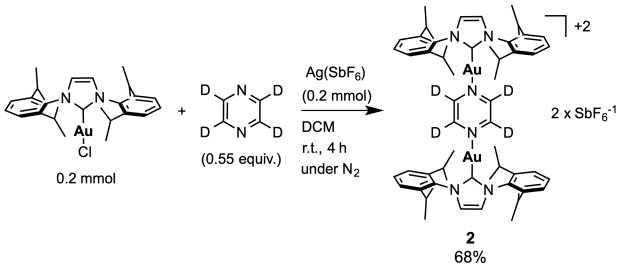

Single Crystal X-Ray Diffraction of 1 and 2. Single-crystal XRD measurements confirmed the expected encapsulating structure of the NHC Cu(I) rotor complex **1**. The NHC Cu(I) complex **1** crystallized in the monoclinic space group $P2_1/c$ with four molecules per unit cell (Z=4) (Table S1). Several key structural parameters are described in Figure 2c. The concave-shaped IPr-NHC ligand having a cone angle of ca. 164º, as evaluated by the Tolman cone angle definition, was

coordinated to the Cu(I) atom with a distance of 1.873(2) Å ($l_{M\text{-}NHC}$) (Figure 2c and d)[23]. The pyrazine rotator was coordinated to the two Cu(I) metals with the same length of 1.896(2) Å from either pyrazine nitrogen to the Cu(I) center ($l_{M\text{-}Py}$). The NHC carbene carbon, the Cu(I) atoms, and the pyrazine rotator were slightly bent (ca. 6.0 º) but co-linearly arranged, as though the transition metal had been implanted into the rotational axis with a total length ($l_{M\text{-}NHC}$ + $l_{M\text{-}Py}$) of 3.769 Å (Figure 2d and S2a). The dihedral angle θ between the NHC plane and the pyrazine ring was 15.5º, showing that the rotator was slightly rotated from the plane of the NHC (Figure 2d and e). The SbF_6^{-1} anions were positioned between the diisopropylbenzene substituents of the alpha and beta side of NHC ligands in a molecule with having a distance of 2.505 Å from the closest proton of the isopropyl moiety of the NHC ligand to the fluorine atom of the SbF_6^{-1} anion. Additionally, the anions have a distance of 2.917 Å from the closest fluorine atom of the anion to the pyrazine plane, which are relatively faraway from the bridging pyrazine rotator as compared to that of mononuclear Cu(I) cationic complex bearing the NHC moiety and pyridine as ligands (Figure 2e and S2b)[27]. The observed geometries of anions near the Cu(I) complex **1** indicated that access of the anions to the central rotator was obstructed by the bulkiness of the NHC ligands, which provided local volume for motion of the rotator to occur.

The crystal structure of the NHC Au(I) rotor complex **2** was also obtained by single-crystal XRD, and the structure was very similar with that of crystal **1** (Figures 2f–g and S3). The Au(I) complex **2** was packed in the space group $P2_1/c$, and the structure of the metal complex with packing manner of the SbF_6^{-1} anions was homologous to that of the Cu(I) complex **1** (Figures 2f–g, S3b, and Table S1). Geometry parameters $l_{M\text{-}NHC}$, $l_{M\text{-}Py}$, and θ of the Au(I) complex **2** showed differences from those of the Cu(I) complex **1**. The $l_{M\text{-}NHC}$ and $l_{M\text{-}Py}$ of the Au(I) complex **2** were 1.95(2) Å and 2.04(1) Å, respectively, indicating that the length of rotational-axis ($l_{M\text{-}NHC}$ + $l_{M\text{-}Py}$) was ca. 0.2 Å longer than that of the Cu(I) complex **1**, reasoned by the larger van der Waals radius of Au than Cu atom. A larger dihedral angle θ was observed for the Au(I) complex **2** (20.7º) than that of the Cu complex **1** (15.5º, Figure 2f–g and Table 1).

Single-crystal XRD measurements between 195 K to 350 K, with four intermediate points at 250, 275, 300, and 325 K (Figure S4–6 and Table S1), revealed no significant structural changes and, similarly, differential scanning calorimetry (DSC) profiles in the range 195–350 K showed no significant peaks indicating that the crystals **1** and **2** have no thermally triggered phase transitions (Figure S7).

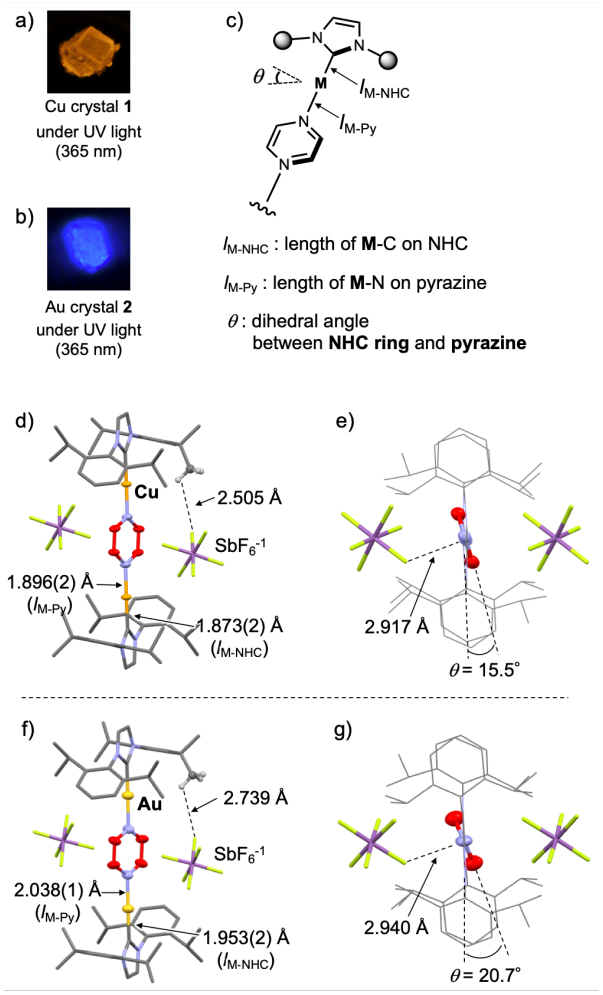

Figure 2. Photographs of a) the Cu(I) crystal 1 and b) Au(I) crystal 2 taken under UV light. c) Line formula with the definition of key structural parameters. Crystal structures of d) 1 and f) 2 with the NHC ligands shown in stick bar and pyrazine rotator highlighted in red. Structure view from the top of rotation-axis of rotor e) 1 and g) 2.

Table 1. Key crystal structural parameters of the NHC rotor 1 and 2.

samples	$l_{M\text{-}Py}$ / Å	$l_{M\text{-}NHC}$ / Å	θ / º
1 at 275 K	1.896(2)	1.873(2)	15.5
1 at 350 K	1.895(2)	1.871(2)	15.1
2 at 275 K	2.04(1)	1.95(2)	20.7
2 at 350 K	2.04(1)	1.96(1)	20.5

Characterization of Rotational Dynamics by Variable Temperature Solid-State ^{2}H NMR.

In order to investigate the rotational dynamics of the pyrazine-d_4 rotator in crystals of NHC complexes **1** and **2**, we carried out variable temperature solid-state (SS) ^{2}H NMR spin-echo measurements that were followed by line shape simulations. It has been established that the method is ideally suited to determine the dynamics of deuterium-enriched moieties with site-

exchange rates in the dynamic range of ca. 10^4–10^7 s^{-1} [28]. Figures 3a and b show the experimental spectra (solid black lines) measured in the temperature range between 340 K and 275 K. Simulated SS ^{2}H NMR spectra (solid red lines) were obtained using a quadrupolar coupling constant (QCC) of 110 kHz, a cone angle of 60° formed between the rotational 1,4-axis and C-D bond vector of the pyrazine, a 10% or 15% static contribution, and a log-Gaussian distribution of the rotational jumping rates having a width □ = 0.5 with Brownian jumps of 180° in agreement with the crystal structures (Figure 3c and S8)[28].

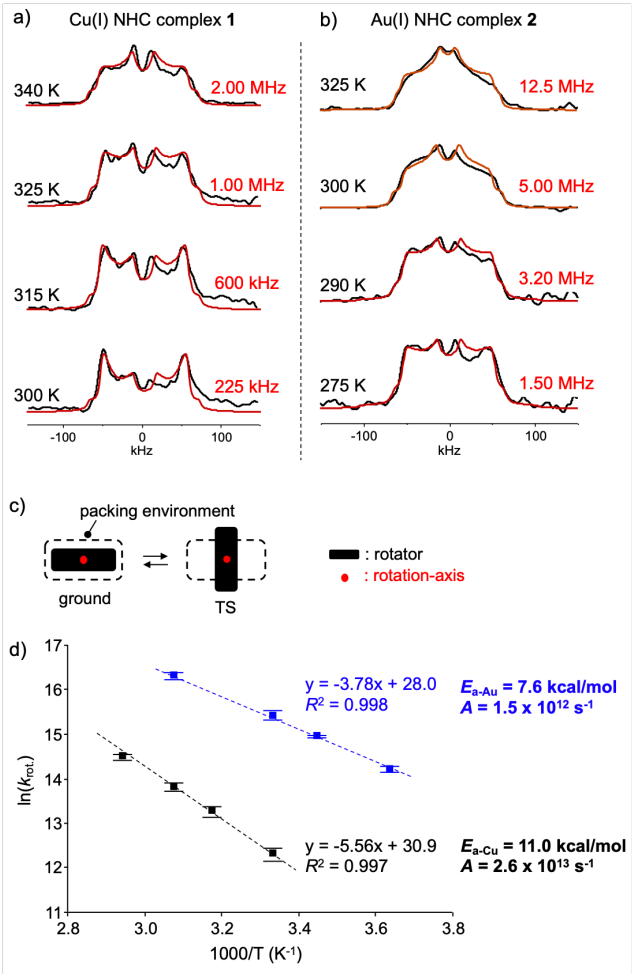

Figure 3. Variable temperature (VT) solid-state (SS) NMR studies of crystals 1 and 2. Experimental SS ^{2}H NMR spectra of a) the Cu(I) rotor 1 and b) the Au(I) rotor 2 represented in solid black line, and the simulated spectra illustrated in red dashed line. c) Representation of the ground and transition states of 2-fold rotation in solid-state. d) Arrhenius plot containing error bar with evaluated energy barrier (E_a) and pre-exponential factor (A) of pyrazine rotator dynamics in crystal 1 and 2 described in black and blue, respectively.

The calculated line shapes provided a reasonable match with the experimental spectra, with the Cu(I) complex **1** experiencing dynamics in the intermediate exchange regime as given by a simulated rotational frequency of 2.00 MHz at 340 K. Further measurements at 325, 315, 300 K were simulated with rotational exchange frequencies ($k_{rot.}$) centered at 1.00, 0.60, and 0.23 MHz, respectively (Figure 3a). By contrast, the spectra of Au(I) complex **2** measured at 325, 300, 290, and 275 K were simulated with k_{rot} values centered at 12.5, 5.00, 3.20, and 1.50 MHz, which are clearly greater than those of the Cu(I) complex **1**. Accordingly, the Arrhenius plots constructed from the $k_{rot.}$ of **1** and **2** presented a significant difference in the corresponding activation energy ($E_{a\text{-}Cu}$ and $E_{a\text{-}Au}$). As shown in Figure 3d, the Cu(I) complex **1** showed an $E_{a\text{-}Cu}$ = 11.0 kcal/mol and a pre-experimental factor A = 2.6 x 10^{13} s^{-1}. In contrast, results from the Au(I) rotor **2** revealed $E_{a\text{-}Au}$ = 7.6 kcal/mol and A = 1.5 x 10^{12} s^{-1}. The calculated A values for both compounds are consistent with the values observed for phenylene rotators in several dumbbell-shaped molecular rotors (ca. 10^{10}–10^{14} s^{-1})[2b]. We note that the line shapes of both complexes measured above 275 K were reasonably well characterized by a simple 180° site exchange model approaching the fast exchange regime.

Investigation into the Origin of Energy Difference in Activation Barriers between Rotor 1 and 2. In order to understand the rotational dynamics of NHC Cu(I) rotor **1** and Au(I) rotor **2**, we carried out DFT calculations using Intramolecular Symmetry-Adapted Perturbation Theory (I-SAPT)[29] and Natural Bond Orbital (NBO) analysis[30,31] to gain insights, respectively, into their steric and electronic effects. As illustrated in Figure 4a, we considered that steric repulsion between the rotator and the NHC ligand should increase the energy of the rotational transition state while □-back donation from the filled *d* orbitals of the metal to the □* orbitals of the rotator should stabilize it. We hypothesized that Au(I) rotor **2** would experience a weaker steric effect and a stronger □-back donation than those of Cu(I) rotor **1** because of the longer length of the rotational axis and the relatively large size of *d* orbitals of the Au(I) atom (Figure 4a).

To obtain geometries and energy values for the rotational ground and transition states (TS) we took the initial geometries of both NHC bimetal cationic complexes from the crystal structures, followed by optimizing the positions of H atoms by fixing the geometries of heavy atoms using DFT calculation with B3LYP/6-31G level[32]. To avoid complication on the calculations and further analysis, the counter anions were omitted. The geometry-optimized ground states were calculated using □B97XD/6-31G(d) for organic atoms and LanL2DZ for metals with all but the carbons and hydrogen atoms of the pyrazine rotator fixed in order to simulate the rigidity of the local rotator environment[32]. The TS for the 2-fold rotation of rotors **1** and **2** were obtained by the Locally Updated Planes (LUP) method, one of the conventional path optimization calculations using the GRRM17 program[33-35]. The atoms on the NHC ligands and metals were fixed, and the calculation for the TS set at the same level as that used for the ground state.

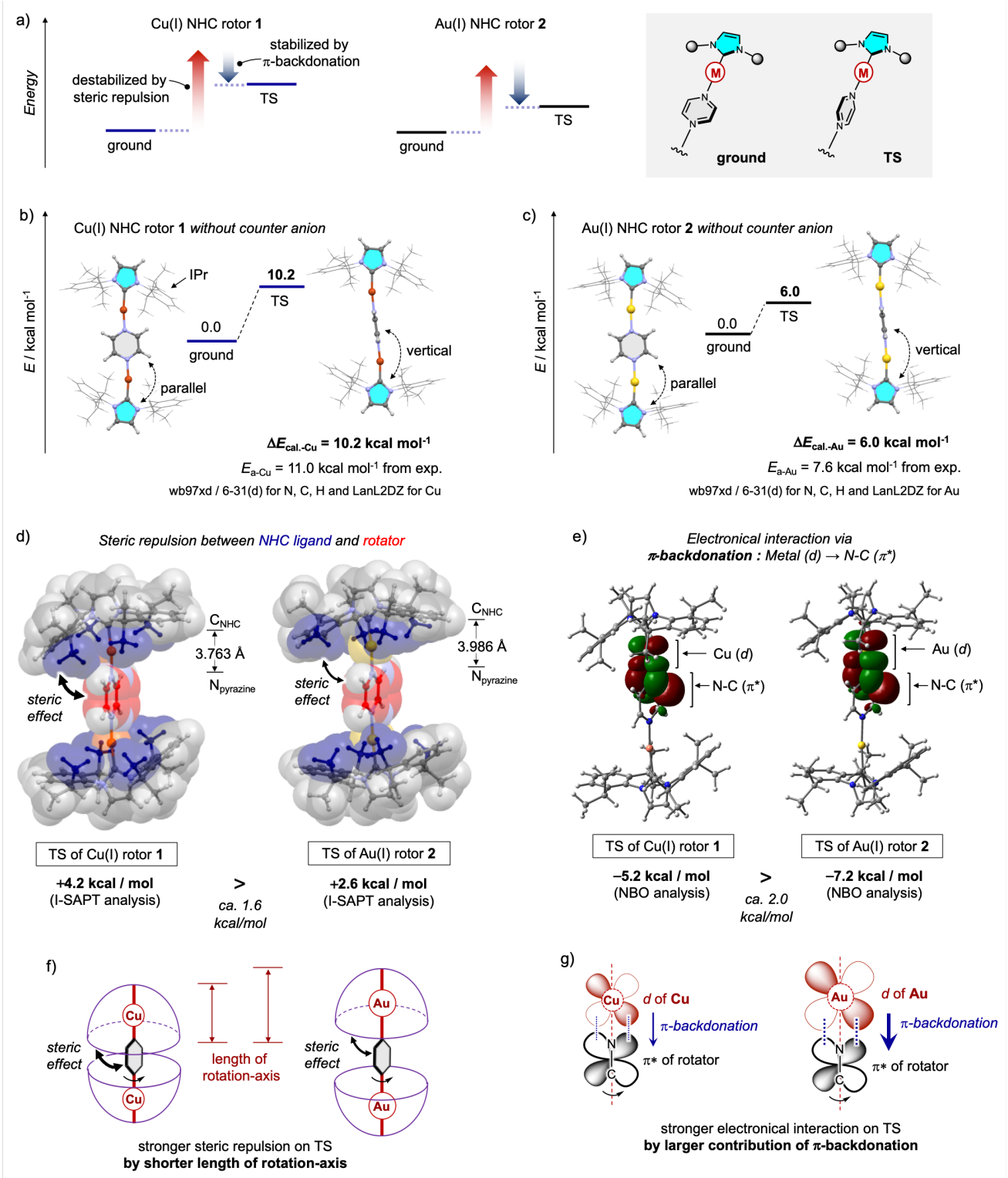

Figure 4. DFT calculations with NBO and SAPT analysis of rotor 1 and 2. a) Illustration of qualitative trends of steric and π-back donation on the energies of the ground and transition state for 2-fold rotation for Cu(I) rotor 1 and Au(I) rotor 2. Calculated energy diagrams and the obtained structural geometries of ground-state and TS of b) Cu(I) rotor 1 and c) Au(I) rotor 2. d) Evaluated steric repulsive interactions on TS for rotor 1 (left) and 2 (right) using I-SAPT analysis and the TS geometries illustrated in the space-filling model. e) Estimated electronic interaction via π-back donation from *d* of metals to π* of pyrazine for rotor 1 (left) and 2 (right). Representation of f) steric repulsion and g) π-back donation effect near the rotator as well as the difference between Cu and Au on the rotation-axis.

The calculated ground-state geometries of rotors **1** and **2**

were analogous to those obtained from the single crystal XRD, and the calculated energy barriers qualitatively matched the tendency observed from the ^{2}H-SS-NMR analyses. The optimized ground-state geometries of the two rotors showed that the pyrazine rings were slightly tilted from the NHC planes with dihedral angles θ *of* ca. 6.0–7.0º, which were ca. 10º smaller than those observed in the crystal structures (Figures 4b–c and S9–10).). One possible difference for these geometry differences may be the omission of the counter anions during the calculations. Transition state calculations indicated that the pyrazine rotators are orthogonal to the planes of the NHC (β = ca. 90º), with the greatest steric congestion occurring between the isopropyl groups on the ligands and the rotator (Figures 4b and c). The calculated energy barriers for the rotations were 10.2 kcal/mol for the Cu(I) rotor **1** ($\Delta E_{cal.-Cu}$) and 6.0 kcal/mol for the Au(I) rotor **2** ($\Delta E_{cal.-Au}$), respectively. The ca. 4.0 kcal/mol of higher energy barrier of the Cu(I) rotor **1** is consistent with the experimental activation energies determined by SS-NMR studies, although the calculated values are ca. 1.0 kcal/mol lower (Figures 4b and c). We propose that the difference between the SS ^{2}H NMR experiments and calculations may originate from steric interactions with the SbF_6^- [1]anions, which were omitted in the calculations.

As seen in the crystal structures, changing the metal from Cu to Au increased the length of the rotation-axis by ca. 0.2 Å, which is expected to cause a smaller steric effect in the case of Au (I) rotor **2.** Steric effects quantitatively evaluated by the I-SAPT analysis method using the TS geometries (Figure 4d and S13) indicated that calculated repulsive interactions in Cu(I) rotor **1** and Au(I) rotor **2** were 4.2 kcal/mol and 2.6 kcal/mol, respectively (Figure 4d and Table S2).

As shown by the NBO analysis of the transition states for both rotors in Figure 4e, the stabilization via the π-back donation from *d* orbitals of the metals to a π^*orbital of the pyrazine rotator gives energy values of –5.2 kcal/mol for Cu(I) rotor **1** and –7.2 kcal/mol for Au(I) rotor **2** (Figure S11–12). Calculations indicated that the Au(I)rotor **2** has a larger *d* orbital as well as more *d* and π^* overlap than those of the Cu(I) rotor **1**.

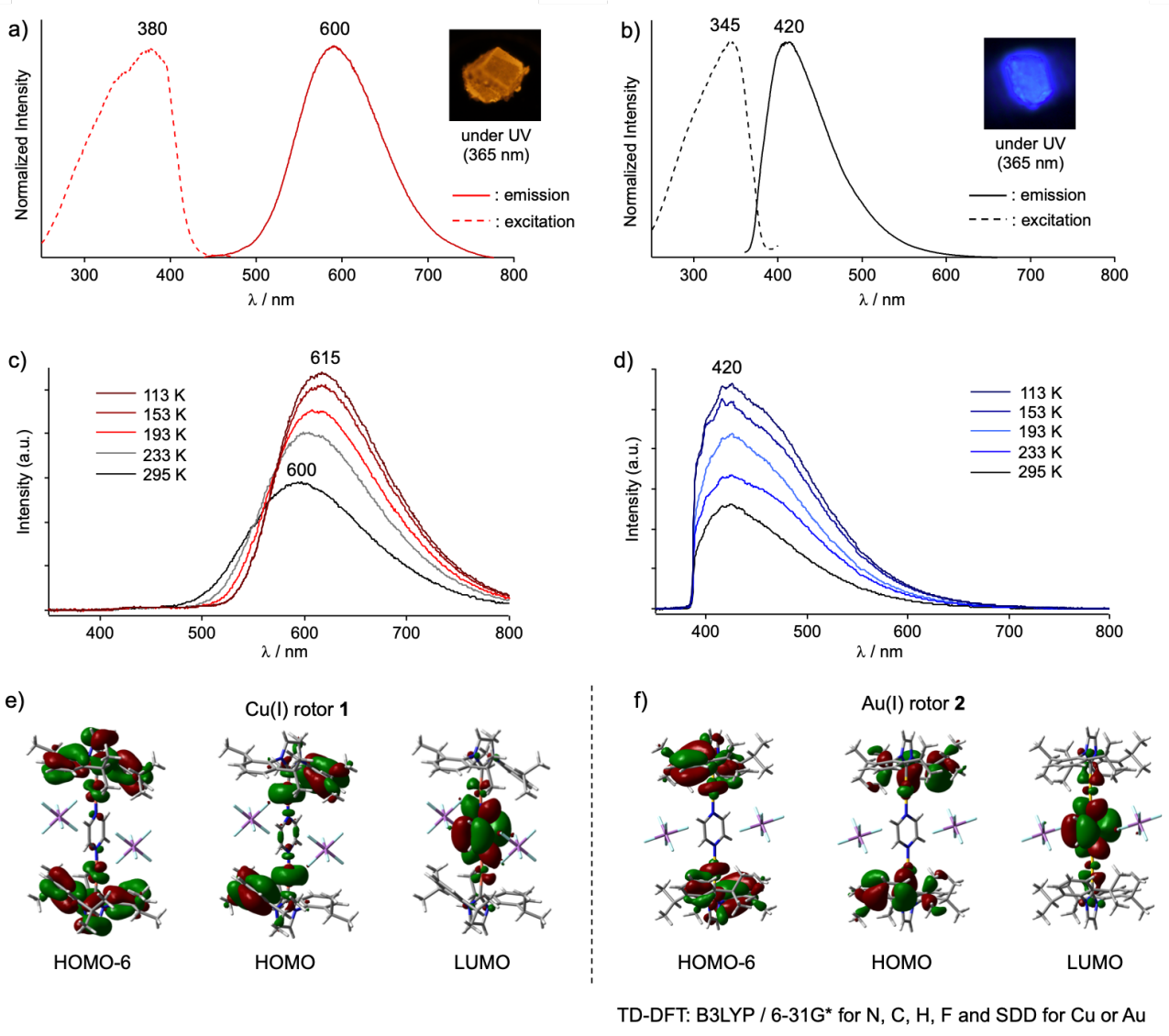

Figure 5. Emission and excitation spectra of the crystal a) 1 and b) 2. Emission spectra of crystal c) 1 and d) 2 under UV (365 nm) irradiation as a function of temperature ranging 113-295K. Frontier molecular orbitals obtained by TD-DFT calculation of the Cu(I) rotor e) 1 and the Au(I) rotor f) 2 in crystals.

These results suggest that stabilization via π-back donation in the TS can be one of the major factors for determining the rotational barriers, and the magnitude can be enhanced by changing metals on the rotation-axis from Cu to Au. To evaluate the electronic stabilization on the TS geometry in a different way, we investigated the ground and transition states for the rotation of model rotor complexes with less steric hindrance by introducing methyl groups instead of bulky 2,6-diisopropylphenyl groups on the NHC rings (Figure S14). Notably, the orthogonal conformation between pyrazine and NHC ring goes from being the rotational transition state geometry in the bulky NHC rotors **1** and **2**, to become the ground state in the non-sterically encumbered models of both Cu(I) and Au(I) rotors. NBO analysis of these geometries indicated that the Au(I) rotor has 2.8 kcal/mol larger stabilization energy via the π-back donation than the Cu(I) rotor. This difference in the electronic stabilization effect for model complexes of Cu(I) and Au(I) have the same trend as those observed in the actual bulky complexes (Figure S15). The *d* orbitals interactions with the NHC ligands were ca. 8–16 kcal/mol stronger than those between the metals and the pyrazine, as evaluated by further NBO analysis of both the actual and modeled rotors. Based on these results, we interpret that the ca. 4.0 kcal/mol lower rotational barrier of the Au(I) rotors is the result of ca. 1.6 kcal/mol of the weaker steric repulsive interactions and ca. 2.0 kcal/mol of the stronger stabilization on the TS by the π-back donation (Figure 4a, f–g). These analyses suggest that our design strategy based on the encapsulating NHC metal complexes does make it possible to modulate the stabilization effect from the π-back donation from the metals to the rotator. Unfortunately, a simple numerical analysis of the calculated rotation barriers ($\Delta E_{cal.-Cu}$ and $\Delta E_{cal.-Au}$) cannot be obtained from the energies derived from steric (I-SAPT) and π-back donating interactions (NBO) because of the different calculation methods as well unaccounted lattice contributions (Figure S16 for details).

Solid-State Emission Properties of Rotor 1 and 2. One of the most interesting observations of this work is that an extremely weak emission in solution becomes quite strong in the solid state. This is a feature of many aggregation-induced emission systems that have been shown to display motion-dependent excited state deactivation. Considering that the time constant for emission in the solid state is in the time regime for rotation, it seems likely that rotational motion may be involved in processes that deactivate the excited state by going through a conical intersection. Recently, pioneering examples of luminescent amphidynamic crystals have demonstrate remarkable control of solid-state emission based on molecular rotation-induced emission quenching[13,14,37]. Also shown in Figures 5a–b, crystals of Cu(I) rotor **1** and Au(I) rotor **2** exhibited significantly different emission, red and blue, respectively, under irradiation with UV light (λ_{ex} = 365 nm) at room temperature. As mentioned above, the emissions of **1** and **2** in CH_2Cl_2 solutions were very weak as compared to those in the solid-state. Relatively high quantum yields (Φ) as 0.14 for crystal **1** and 0.12 for crystal **2** suggest that their emission properties are determined by their aggregated structures (Table S3 and Figure S17–19)[36]. Crystals of Cu(I) rotor **1** showed a broad emission with maximum intensity ($\lambda_{em.max}$) at 600 nm, and a broad excitation band with a peak ($\lambda_{ex.max}$) at 380 nm (Figure 5a). On the other hand, crystal **2** exhibited the blue-shifted excitation and emission spectra with shorter $\lambda_{ex.max}$ at 345 nm and $\lambda_{em.max}$ at 420 nm (Figure 5b). This trend was also documented with time-dependent (TD) DFT calculations using the single-crystal XRD structures of **1** and **2** at room temperature as the input for the calculations (Figure S21). The calculated excitations exhibit qualitatively good agreement with the measured $\lambda_{ex.max}$ of the excitation spectra (Figure S21), and the contributed molecular orbitals were identified as transitions from HOMO and HOMO-6 to LUMO (Figures 5e–f and Tables S4–5). The LUMOs of both rotors mainly consisted of orbitals on the pyrazine and partial Cu or Au metal participations, as shown in Figures 5e and f. The HOMO and HOMO-6 of Cu(I) rotor **1** were distributed over the pyrazine and imidazole planes with Cu(I) atoms on the rotation-axis. In contrast, those orbitals in Au(I) rotor **2** were majorly localized on the NHC ligands and Au(I) atoms where orbitals in the pyrazine moiety were scarcely contributed (Figures 5e–f and Tables S4–5). These results of the TD-DFT calculation studies indicated that photoexcitation states of both crystalline rotors can be characterized as ligand-to-ligand with metal charge transfer involvement. The more largely delocalized HOMO and HOMO-6 of Cu(I) rotor **1** as compared to that of the Au(I) rotor **2** might explain the red-shifted excitation and emission bands in the former.

Crystals of Au(I) rotor **2** exhibited a significant and reversible emission enhancement by lowering temperature from 295 K to 153 K (Figure 5d). An emission decay measured at room temperature was fitted using a double exponential function with varying pre-exponentials for the short- (ca. 0.4 μs) and long-lived components (ca. 1.0 μs), which were used to calculated a weighted average lifetime ($\tau_{av.}$) of 0.87 μs (Table S3 and Figure S19), indicating the involvement of excited triplet states in the emission process. We note that the rotational dynamics of the pyrazine rotator slowed down significantly in the same temperature range, and that phosphorescence occurs in a similar time scale as molecular the rotations (ca. 0.3 μs for the Au(I) rotor **2** at room temperature). Additionally, changes in the ratio of the emission intensity $I_{max,T}/I_{max,295K}$ between 295 K to 113 K of crystal **2** as a function of temperature indicated that the greatest changes in emission intensity occur in the range of 295 K to 153 K, where molecular rotations are more greatly affected, rather than in the interval between 153 K to 113K (Figure 5d and S20) where rotations may be much slower than the time it takes for the excited state to decay. In our previous luminescent Au(I)-aryl complexes with amphidynamic properties we showed that arylene rotations induced efficient emission quenching because changes in the geometry of chromophore induces changes in the excited and ground electronic states[13,14]. We suggest that the observed emission enhancement of Au(I) rotor **2** may also correlate with the suppression of molecular rotation at lower temperature[13,14,37].

The emission enhancement of crystal **1** by the lowering the sample temperature was also observed, and the change in the ratio of emission intensity $I_{max,T}/I_{max,295K}$ between 295 K to 113 K of crystal **1** showed a trend that is similar to that observed with crystal **2** (Figure 5c and S20). The weighted average lifetime for emission decay measured at room temperature was

calculated to be 3.06 μs of τ_{av} from a double exponential function with components of ca. 1.7 μs and 19.0 μs and their corresponding pre-exponentials (A_n) (Table S3). The μs scale of emission decay was near the pyrazine rotation time scale (ca. 5.0 μs for the Cu(I) rotor **1**), indicating that conformational changes via the rotation may increase the rate of a nonradiative pathway, as observed in the Au(I) rotor **2**. We note that a ca. 15 nm red shift in the emission maximum of crystal **1** observed upon cooling the sample was not observable in crystals of **2**, even though our microscope optics truncate the blue-edge of the spectrum. Possible reasons for the red-shifted phosphorescence emission of Cu(I) rotor **1** may include structural relaxations as a function of temperature, or to the participation of thermally activated delayed fluorescence (TADF) at higher temperatures, [38] which will require additional analysis.

Conclusion

We described here a novel platform of crystalline molecular rotors by utilizing the concave-shield of NHC groups with implanted transition metals (Cu or Au) on the rotation-axis. The crystalline rotors were constructed from bulky *N*-heterocyclic carbene (NHC) ligand as an encapsulating stator, deuterated pyrazine as the rotator having π-accepting ability, and Cu(I) or Au(I) metals as a center of the axle. The designed encapsulating NHC rotors are easier to synthesize compared to previously reported enclosed gyroscopic rotors, and scarcely depended on the crystal structures, which are crucial features for an encapsulating, dumbbell type design. The rotational barriers were reasonably modulated by changing the metals on the axle, which routed from steric repulsive interactions near the rotator and electronic interaction on the TS via π-back donation from the metal to the rotator. DFT calculations revealed that altering the metals from Cu to Au results in both the elongation of rotation-axis, reducing the steric hindrance, and the largely overlapped d–π^* orbitals yielding stronger π-back donation, which lower energy barrier. The difference in electronic delocalization between the Cu(I) and Au(I) rotors yielded distinct emission colors in solid-state. Both crystalline rotors exhibited emission lifetimes on the μs time scale, which could be quenched by the molecular rotations occurring near the time scale. A broad library of NHC ligands including bulky structures have already been developed with the aim at controlling steric and electronic effects near the metal-center space. Thus, many NHC metal complex-based molecular rotors can be developed to demonstrate a similarly broad range of rotational dynamics and fine-control of rotational barriers in solid-state. Our results reveal a general way to use these abundant ligands as functional stators and the metal-ligand coordination bonds as an adjustable rotation-axis for amphidynamic crystals. This platform will enable the further study on these exotic materials, which have both high structural integrity and high mobility of the molecular components, and greatly enhance the development of new functional materials based on the molecular dynamics change in the static crystalline solid.

ASSOCIATED CONTENT

Supporting Information

Spectroscopy, X-ray crystal graphic, thermal analysis, quantum chemical calculation data, Supporting movies and other additional information. This material is available free of charge via the Internet at http://pubs.acs.org.

AUTHOR INFORMATION

Corresponding Authors

Mingoo Jin (mingoo@icredd.hokudai.ac.jp)
Hajime Ito (hajito@eng.hokudai.ac.jp)

Present Addresses

†, ‡ Kita 13 Nishi 8 Kita-ku, Sapporo, Hokkaido, 060-8628, Japan
¶ 607 Charles E. Young Drive East, Los Angeles CA 90095-1569, USA

Author Contributions

The manuscript was written through contributions of all authors. All authors have given approval to the final version of the manuscript.

Notes

ORCIDs of the authors
Mingoo Jin: 0000-0001-6199-8802
Hajime Ito: 0000-0003-3852-6721
Miguel A. Garcia-Garibay: 0000-0002-6268-1943

ACKNOWLEDGMENT

This work was financially supported by the MEXT (Japan) program "Strategic Molecular and Materials Chemistry through Innovative Coupling Reactions" of Hokkaido University; Building of Consortia for the Development of Human Resources in Science and Technology, "Program for Fostering Researchers for the Next Generation"; and by JSPS KAKENHI grants JP17H06370, JP18H03907 and JP19K23618. We thank Dr. Suzuki K. and Mr. Ozawa Y. for their valuable comment and discussion for the computational studies. Work at UCLA was supported by NSF Grants DMR-1700471 and MRI-1532232 (Solid-State NMR).

REFERENCES

(1) Garcia-Garibay, M. A. Nanoscale gadgets. *Nat. Mater.* **2008**, *7*, 431–432.

(2) (a) Vogelsberg, C. S. & Garcia-Garibay, M. A. Crystalline molecular machines: function, phase order, dimensionality, and composition. *Chem. Soc. Rev.* **2012**, *41*, 1892–1910. (b) Howe, M.E. & Garcia-Garibay, M. A. The Roles of Intrinsic Barriers and Crystal Fluidity in Determining the Dynamics of Crystalline Molecular Rotors and Molecular Machines. *J. Org. Chem.* **2019**, *84*, 9835–9849.

(3) Bracco, S., Comotti, A. & Sozzani, P. Molecular rotors built in porous materials. *Acc. Chem. Res.* **2016**, *49*, 1701–1710.

(4) Catalano, L. & Naumov, P. Exploiting rotational motion in molecular crystals. *CrystEngComm.* **2018**, *20*, 5872–5883.

(5) Gonzalez-Nelson, A., Coudert, F.X. & van der Veen, M. A. Rotational dynamics of linkers in metal-organic frameworks. *Nanomaterials* **2019**, *9*, 330.

(6) Chung, H., Dudenko, D., Zhang, F., D'Avino, G., Ruzie, C., Richard, A., Schweicher, G., Cornil, J., Beljonne, D., Geerts, Y. & Diao, Y. Rotator side chains trigger cooperative transition for shape and function memory effect in organic semiconductors. *Nat. Commun.* **2018**, *9*, 278.

(7) Setaka, W. & Yamaguchi, K. Order–Disorder transition of dipolar rotor in a crystalline molecular gyrotop and its optical change. *J. Am. Chem. Soc.* **2013**, *135*, 14560–14563.

(8) Yao, Z. S., Yamamoto, K., Cai, H. L., Takahashi, K. & Sato, O. Above room temperature organic ferroelectrics: Diprotonated 1,4-

Diazabicyclo[2.2.2]octane shifts between two 2-chlorobenzoates. *J. Am. Chem. Soc.* **2016**, *138*, 12005–12008.

(9) Yao, Z. S., Mito, M., Kamachi, T., Shiota, Y., Yoshizawa, K., Azuma, N., Miyazaki, Y., Takahashi, K., Zhang, K., Nakanishi, T., Kang, S., Kanegawa, S. & Sato, O. Molecular motor-driven abrupt anisotropic shape change in a single crystal of a Ni complex. *Nat. Chem.* **2014**, *6*, 1079–1083.

(10) Su, S. Q., Kamachi, T., Yao, Z. S., Huang, Y. G., Shiota, Y., Yoshizawa, K., Azuma, N., Miyazaki, Y., Nakano, M., Maruta, G., Takeda, S., Kang, S., Kanegawa, S. & Sato O. Assembling an alkyl rotor to access abrupt and reversible crystalline deformation of a cobalt(II) complex. *Nat. Commun.* **2015**, *6*, 8810.

(11) Colin-Molina, A., Karothu, D. P., Jellen, M. J., Toscano, R. A., Garcia-Garibay, M. A., Naumov, P. & Rodriguez-Molina, B. Thermosalient amphidynamic molecular machines: Motion at the molecular and macroscopic scales. *Matter.* **2019**, *1*, 1033–1046.

(12) Jiang, X., Duan, H. B., Khan, S. I. & Garcia-Garibay, M. A. Diffusion-controlled rotation of triptycene in a Metal-Organic Framework (MOF) sheds light on the viscosity of MOF-confined solvent. *ACS Cent Sci.* **2016**, *2*, 608–613.

(13) Jin, M., Chung, T. S., Seki, T., Ito, H. & Garcia-Garibay, M. A. Phosphorescence Control Mediated by Molecular Rotation and Aurophilic Interactions in Amphidynamic Crystals of 1,4-Bis[tri-(*p*-fluorophenyl)phosphane-gold(I)-ethynyl]benzene. *J. Am. Chem. Soc.* **2017**, *139*, 18115–18121.

(14) Jin, M., Yamamoto, S., Seki, T., Ito, H. & Garcia-Garibay, M. A. Anisotropic Thermal Expansion as the Source of Macroscopic and Molecular Scale Motion in Phosphorescent Amphidynamic Crystals. *Angew. Chem. Int. Ed.* **2019**, *58*, 18003–18010.

(15) Nuñez, J. E., Natarajan, A., Khan, S. I. & Garcia-Garibay, M. A. Synthesis of a Triply-Bridged Molecular Gyroscope by a Directed Meridional Cyclization Strategy. *Org. Lett.* **2007**, *9*, 3559–3561.

(16) Lang, G. M., Shima, T., Wang, L., Cluff, K. J., Skopek, K., Hampel, F., Blümel, J. & Gladysz, J. A. Gyroscope-like complexes based on dibridgehead diphosphine cages that are accessed by threefold intramolecular ring-closing metatheses and encase $Fe(CO)_3$, $Fe(CO)_2(NO)^+$, and $Fe(CO)_3(H)^+$ rotators. *J. Am. Chem. Soc.* **2016**, *138*, 7649–7663.

(17) Gould, S. L., Tranchemontagne, D., Yaghi, O. M. & Garcia-Garibay, M. A. Amphidynamic Character of Crystalline MOF-5: Rotational Dynamics of Terephthalate Phenylenes in a Free-Volume, Sterically Unhindered Environment. *J. Am. Chem. Soc.* **2008**, *130*, 3246–3247.

(18) Vukotic, V. N., Harris, K. J., Zhu, K., Schurko, R. W. & Loeb, S. J. Metal-organic frameworks with dynamic interlocked components. *Nat. Chem.* **2012**, *4*, 456–460.

(19) Danowski, W., Leeuwen, T.V., Abdolahzadeh, S., Roke, D., Browne, W.R., Wezenberg, S.J. & Feringa, B.L. Unidirectional rotary motion in a metal-organic framework. *Nat. Nanotechnol.* **2019**, *14*, 488–494.

(20) Danowski, W. *et al.* Visible-Light-Driven Rotation of Molecular Motors in a Dual-Function Metal-Organic Framework Enabled by Energy Transfer. *J. Am. Chem. Soc.* **2020**, *142*, 9048–9056

(21) Vogelsberg, C. S., Uribe-Romo, F. J., Lipton, A. S., Yang, S., Houk, K. N., Brown, S. & Garcia-Garibay, M. A. Ultrafast rotation in an amphidynamic crystalline metal-organic framework. *Proc. Nat. Acad. Sci.* **2017**, *114*, 13613–13618.

(22) (a) Perego, J., Bracco, S., Negroni, M., Bezuidenhout, C. X., Prando, G., Carretta, P., Comotti, A. & Sozzani, P. Fast motion of molecular rotors in metal-organic framework struts at very low temperatures. *Nat. Chem.* **2020**, *12*, 845–851. (b) Prando, G., Perego, J., Negroni, M., Ricco, M., Bracco, S., Comotti, A., Sozzani, P., Carretta, P. *Nano lett.* **2020**, *20*, 7613–7618.

(23) Gomez-Suarez, A., Nelson, D. J. & Nolan, S. P. Quantifying and understanding the steric properties of N-heterocyclic carbenes. *Chem. Commun.* **2017**, *53*, 2650–2660.

(24) Jazzar, R., Soleilhavoup, M. & Bertrand, G. Cyclic (Alkyl)- and (Aryl)-(amino)carbene Coinage Metal Complexes and Their Applications. *Chem. Rev.* **2020**, *120*, 4141–4168.

(25) Miessler, G. L. & Tarr, D. A. *Inorganic Chemistry 4th Ed.* (Pearson Prentice Hall, 2009)

(26) Comas-Vives, A. & Harvey, J. N. How Important Is Backbonding in Metal Complexes Containing N-Heterocyclic Carbenes? Structural and NBO Analysis. *Eur. J. Inorg. Chem.* **2011**, *2011*, 5025–5035.

(27) Liske, A., Wallbaum, L., Hölzel, T., Föller, J., Gernert, M., Hupp, B., Ganter, C., Marian, C. M. & Steffen, A. Cu–F Interactions between Cationic Linear *N*-Heterocyclic Carbene Copper(I) Pyridine Complexes and Their Counterions Greatly Enhance Blue Luminescence Efficiency. *Inorg. Chem.* **2019**, *58*, 5433–5445.

(28) Macho, V., Brombacher, L. & Spiess, H. W. The NMR-WEBLAB: An internet approach to NMR lineshape analysis. *Appl. Magn. Reson.* **2001**, *20*, 405–432.

(29) Jeziorski, B., Moszynski, R. & Szalewicz, K. Perturbation Theory Approach to Intermolecular Potential Energy Surfaces of van der Waals Complexes. *Chem. Rev.* **1994**, *94*, 1887–1930.

(30) *NBO 7.0,* Glendening, E. D., Badenhoop, J, K., Reed, A. E., Carpenter, J. E., Bohmann, J. A., Morales, C. M., Karafiloglou, P., Landis, C. R. & Weinhold, F. Theoretical Chemistry Institute, University of Wisconsin, Madison (2018).

(31) Glendening, E. D., Landis, C. R. & Weinhold, F. Natural Bond Orbital Methods. *WIREs Comput. Mol. Sci*. **2012**, *2*, 1–42.

(32) *Gaussian 16, Revision B.01*, Frisch, M. J.; Trucks, G. W.; Schlegel, H. B.; Scuseria, G. E.; Robb, M. A.; Cheeseman, J. R.; Scalmani, G.; Barone, V.; Petersson, G. A.; Nakatsuji, H.; Li, X.; Caricato, M.; Marenich, A. V.; Bloino, J.; Janesko, B. G.; Gomperts, R.; Mennucci, B.; Hratchian, H. P.; Ortiz, J. V.; Izmaylov, A. F.; Sonnenberg, J. L.; Williams-Young, D.; Ding, F.; Lipparini, F.; Egidi, F.; Goings, J.; Peng, B.; Petrone, A.; Henderson, T.; Ranasinghe, D.; Zakrzewski, V. G.; Gao, J.; Rega, N.; Zheng, G.; Liang, W.; Hada, M.; Ehara, M.; Toyota, K.; Fukuda, R.; Hasegawa, J.; Ishida, M.; Nakajima, T.; Honda, Y.; Kitao, O.; Nakai, H.; Vreven, T.; Throssell, K.; Montgomery, Jr. J. A.; Peralta, J. E.; Ogliaro, F.; Bearpark, M. J.; Heyd, J. J.; Brothers, E. N.; Kudin, K. N.; Staroverov, V. N.; Keith, T. A.; Kobayashi, R.; Normand, J.; Raghavachari, K.; Rendell, A. P.; Burant, J. C.; Iyengar, S. S.; Tomasi, J.; Cossi, M.; Millam, J. M.; Klene, M.; Adamo, C.; Cammi, R.; Ochterski, J. W.; Martin, R. L.; Morokuma, K.; Farkas, O.; Foresman, J. B. and Fox, D. J., Gaussian, Inc., Wallingford CT, 2016.

(33) *GRRM17*, Maeda, S., Harabuchi, Y., Sumiya, Y., Takagi, M., Suzuki, K., Hatanaka, M., Osada, Y., Taketsugu, T., Morokuma, K., Ohno, K. see http://iqce.jp/GRRM/index_e.shtml (accessed date DAY MONTH, YEAR).

(34) Choi, C. & Elber, R. Reaction Path Study of Helix Formation in Tetrapeptides: Effect of Side Chains, *J. Chem. Phys.* **1991**, *94*, 751–760.

(35) Ayala, P. Y. & Schlegel, H. B. A Combined Method for Determining Reaction Paths, Minima, and Transition State Geometries. *J. Chem. Phys.* **1997**, *107*, 375–384.

(36) Hong, Y., Lam, J. W. Y. & Tang, B. Z. Aggregation-Induced Emission *Chem. Soc. Rev.* **2011**, *40*, 5361–5388.

(37) Li, T. Y., Muthiah Ravinson, D. S., Haiges, R., Djurovich, P. I. & Thompson, M. E. Enhancement of the Luminescent Efficiency in Carbene-Au(I)-Aryl Complexes by the Restriction of Renner-Teller Distortion and Bond Rotation. *J. Am. Chem. Soc.* **2020**, *142*, 6158–6172.

(38) Czerwieniec, R., Leitl, M. J., Homeier, H. H. H. & Yersin, H. Cu(I) complexes–Thermally activated delayed fluorescence. Photophysical approach and material design. *Coord. Chem. Rev.* **2016**, *325*, 2–28.

Insert Table of Contents artwork here

Crystalline molecular rotors

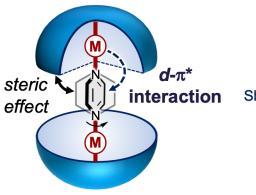

◆ ***concave****-shape NHC ligand*

◆ *rotation-axis* (**C–M–N**) *with implanting* ***transition-metals***

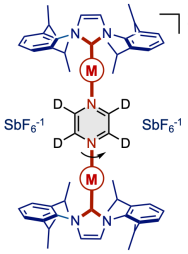

1 [M = Cu(I)]
2 [M = Au(I)]

Cu crystal **1**

under UV light
(365 nm)

Au crystal **2**

under UV light
(365 nm)

*tunable rotation barrier by changing the metal (**Cu** or **Au**) through altering:*
- steric effects via M-L coordination bond length
- electronic effects via strength of π–back donation